Chapter 4

Hydrogen adsorption by graphite intercalation compounds

4.1 Introduction

Understanding the thermodynamics of H_2 adsorption in chemically modified carbons remains an important area of fundamental research. One reason is that physisorption of H_2 by carbons is significantly influenced by dispersion forces, which are notoriously difficult to calculate by first-principles methods. Further, most high-surface-area carbons have disordered structures which are difficult to model by simulations. As discussed in Sec. 1.7, graphite intercalation compounds provide an model system for systematically studying the effects of chemical modification and slit pore spacing on hydrogen adsorption thermodynamics. In this chapter, accurate measurements of the isosteric heat of H_2 adsorption in KC_{24}, RbC_{24}, and CsC_{24} are presented. The effect of alkali-metal doping and graphite interlayer spacing on the adsorption enthalpy are discussed. The effect of adsorption kinetics is also investigated.

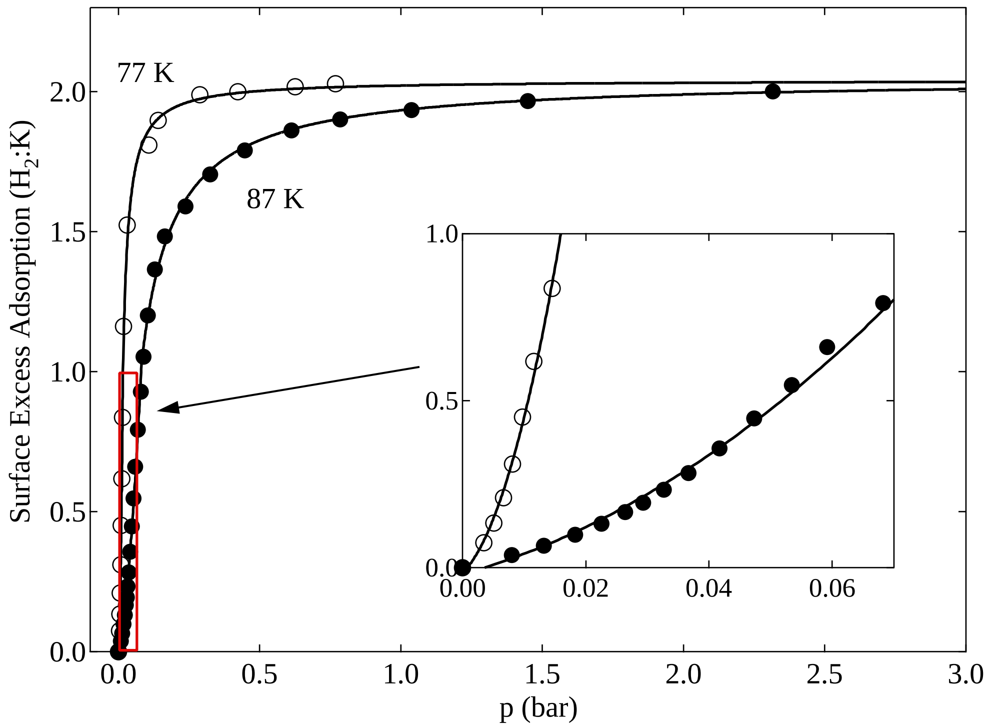

Figure 4.1: Hydrogen adsorption isotherms of KC_{24} at 77 K and 87 K. Inset shows a magnified view of the low-pressure portion of the isotherm contained within the red box. Lines are only a guide for the eye.

4.2 Hydrogen adsorption isotherms of KC_{24}

Hydrogen adsorption isotherms were measured for a 0.787 g sample of KC_{24} synthesized from flake graphite. Loading was done in an argon glovebox so that the sample was not exposed to air at any stage of the experiment. Adsorption isotherms were collected at 77 K and 87 K, and are displayed in Fig. 4.1. The isotherms are steep, and a magnified view of the low-pressure region is provided in the inset. For this sample, the maximum hydrogen composition after adsorption was $KC_{24}(H_2)_{2.03}$, which is equivalent to 1.24 wt%. Both the 77 K and 87 K isotherms reached the same maximum capacity, which is not typically observed for supercritical adsorption in porous carbons [73].

As explained further in Sec. 4.4, adsorption is kinetically limited at a hydrogen com-

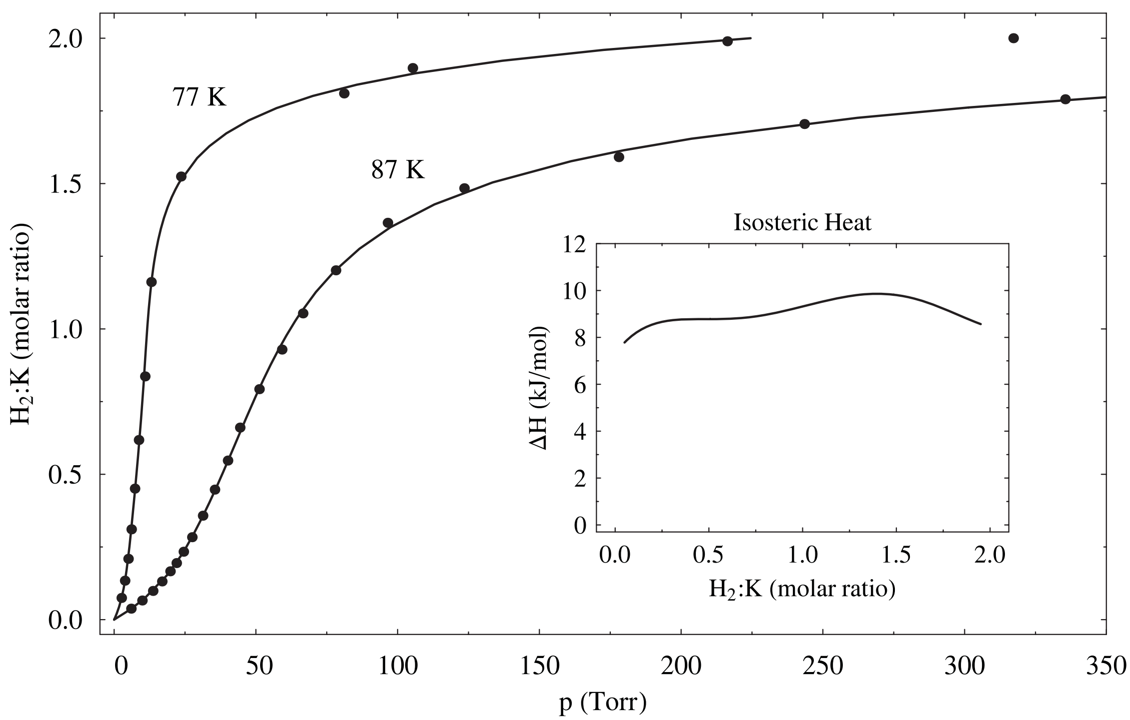

Figure 4.2: Adsorption isotherms of KC_{24} at 77 K and 87 K fitted to a virial-type thermal equation. Inset: Isosteric heat as a function of adsorption amount.

position greater than $KC_{24}(H_2)_{1.6}$, which means that isotherm points in this region do not necessarily correspond to true equilibrium states. At 77 K and 87 K the hydrogen adsorption was fully reversible, and there was not any evidence of dissociation or reaction. Further, there was no reduction in adsorption capacity during three consecutive adsorption/desorption cycles at 77 K. Hydrogen adsorption at 195 K, however, was not completely reversible. When measured after 195 K isotherms, the 77 K isotherms displayed a greatly reduced maximum adsorption capacity. It is very likely that the hydrogen chemically reacted with the potassium intercalant at 195 K [55]. A full characterization of the reaction products was not pursued. It is known that KC_{24} chemisorbs a small amount of hydrogen at elevated temperatures to form a $KC_{24}H_{0.25}$ stoichiometry [47].

The isosteric heat for KC_{24} was calculated from fits of the virial-type thermal equation (Eq. 3.8) to the isotherm data, following the procedure explained in Sec. 3.1.2.3. The

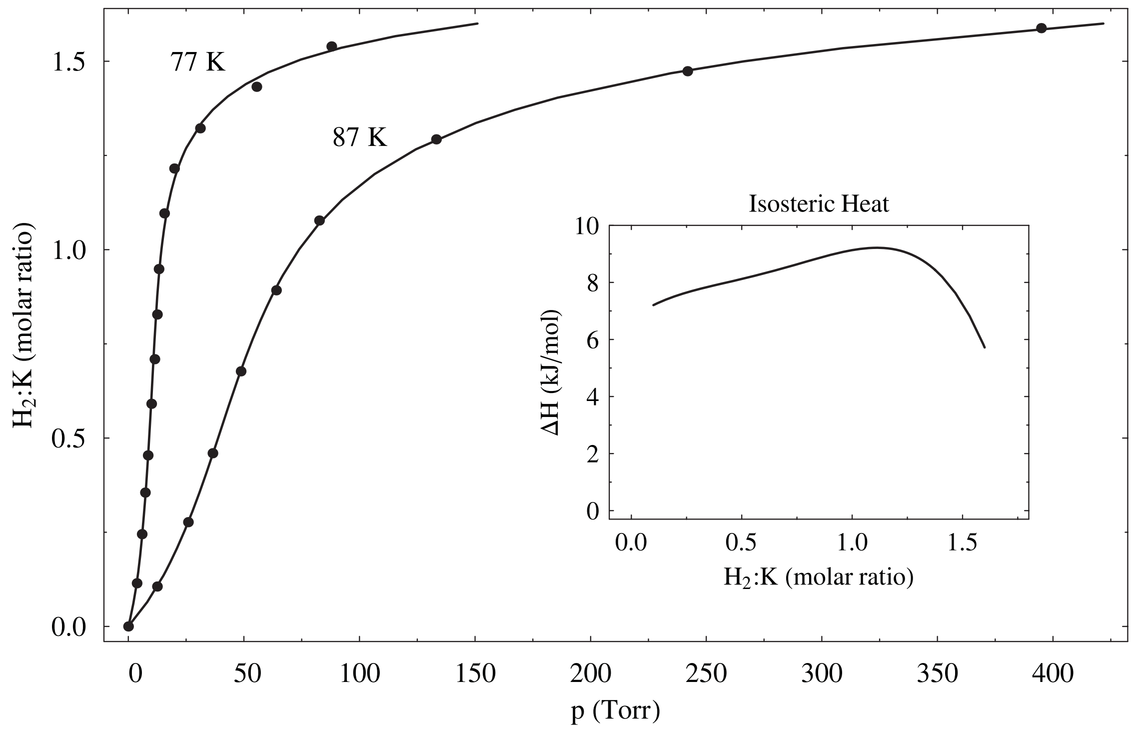

Figure 4.3: Adsorption isotherms of Grafoil-based KC_{24} at 77 K and 87 K fitted to a virial-type thermal equation. Inset: Isosteric heat as a function of adsorption amount.

isotherms, fits, and calculated isosteric heat are displayed in Fig. 4.2. The zero coverage limit of the isosteric heat is $7.3\,\mathrm{kJ\,mol^{-1}}$. The average value of the isosteric heat for $KC_{24}(H_2)_x$ in the range of $0.25 < x < 1.5$ is equal to $9.2\,\mathrm{kJ\,mol^{-1}}$.[1] The detailed shape of the isosteric heat is probably influenced by systematic instrument errors, among other things. The unique "S" shaped curve of the KC_{24} isotherms has been remarked upon previously [48] and is thought to originate from the expansion of the c-axis spacing with H_2 adsorption. Energy losses from mechanical work associated with lattice expansion can be used to explain the anomalous positive slope of the isosteric heat.

Hydrogen adsorption isotherms were also measured for a Grafoil-based KC_{24} sample. The hydrogen adsorption behavior for this sample was markedly different than for the

[1]To be consistent with standard practices in the literature, positive enthalpies are reported throughout the remainder of the thesis, even though the adsorption is exothermic.

Table 4.1: Hydrogen adsorption by alkali metal graphite intercalation compounds

	Max. adsorption[a]		
Sample	wt%	H_2:M	Isosteric heat ($kJ\,mol^{-1}$)[b]
KC_{24}	1.24	2.03	9.2
RbC_{24}	1.03	1.92	12.6
CsC_{24}	0.85	1.79	14.9

[a] Maximum adsorption capacity was measured at 77 K for KC_{24} and at 120 K for RbC_{24} and CsC_{24}.
[b] Isosteric heats were average over H_2:M between 0.25 and 1.5.

flake graphite sample. Measurements were only taken up to a pressure of about 1100 Torr, where the maximum hydrogen composition was $KC_{24}(H_2)_{1.82}$. Adsorption kinetics were much slower at all compositions compared to the flake graphite sample. The adsorption isotherms and calculated isosteric heat are displayed in Fig. 4.3. The isosteric heat follows a physically intuitive pattern. There is an initial increase due to the energy losses in the lattice expansion, followed by a decrease due to the filling of the optimal adsorption sites. The zero coverage enthalpy is only $6.8\,kJ\,mol^{-1}$, while the average isosteric heat between $0.25 < x < 1.5$ is given by $8.5\,kJ\,mol^{-1}$. Interestingly, the average isosteric heat of the Grafoil sample is about $1\,kJ\,mol^{-1}$ smaller than that of the flake graphite sample. The Grafoil used for the synthesis probably had a lower purity than the natural flake graphite. It is possible that surface impurities may have hindered the hydrogen adsorption. Flake graphite GIC samples were used for all future experimental work.

4.3 Hydrogen adsorption isotherms of RbC_{24} and CsC_{24}

Hydrogen adsorption isotherms were collected for RbC_{24} and CsC_{24} samples. These measurements were performed on a Sieverts instrument at NCNR [82]. Temperature control was provided by a closed-cycle helium refrigeration unit, which enabled data to be collected

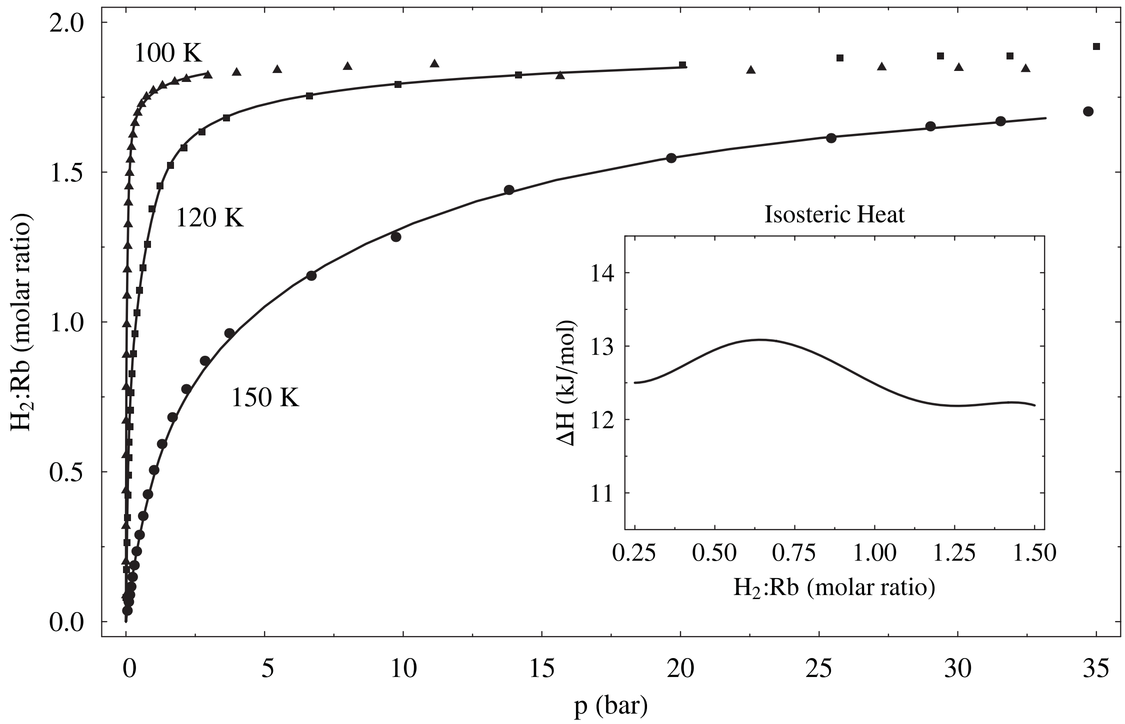

Figure 4.4: Adsorption isotherms of RbC_{24} at 100 K, 120 K, and 150 K fitted to a virial-type thermal equation. Inset: Isosteric heat as a function of adsorption amount.

at temperatures different than the standard 77 K and 87 K. The collection time for each isotherm point was 15 min, regardless of whether equilibrium was reached within that duration. Isotherms for RbC_{24} and CsC_{24} are presented in Fig. 4.4 and Fig. 4.5, respectively.[2] The RbC_{24}, and CsC_{24} isotherms have the classic Langmuir isotherm shape. This reflects the fact that there is apparently no lattice expansion in RbC_{24} or CsC_{24} in response to hydrogen adsorption. For both samples, the largest adsorption amounts were actually obtained at a sample temperature of 120 K. Adsorption at lower temperatures appeared to be reduced due to sluggish kinetics. Isosteric heats for RbC_{24} and CsC_{24}, averaged over $0.25 < x < 1.5$, are an astonishing $12.6\,\mathrm{kJ\,mol^{-1}}$ and $14.9\,\mathrm{kJ\,mol^{-1}}$, respectively. This is close to the optimal adsorption enthalpy of $\Delta H = 18\,\mathrm{kJ\,mol^{-1}}$ for engineering applications

[2] A 77 K isotherm for RbC_{24} and a 100 K isotherm for CsC_{24} were also collected, but are not included in the figures.

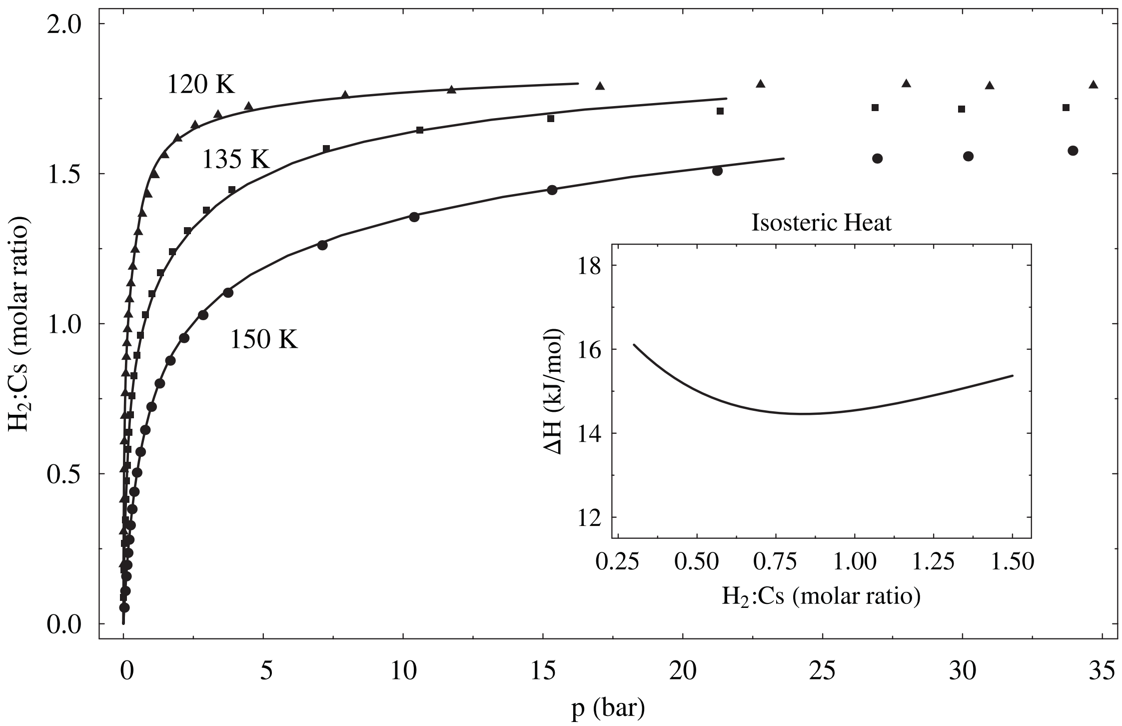

Figure 4.5: Adsorption isotherms of CsC_{24} at 120 K, 135 K, and 150 K fitted to a virial-type thermal equation. Inset: Isosteric heat as a function of adsorption amount.

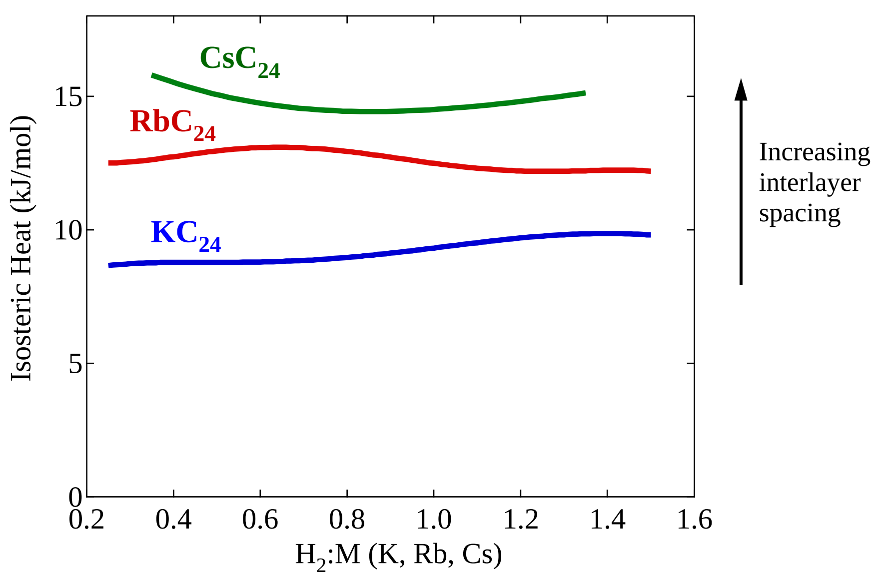

Figure 4.6: Comparison of hydrogen adsorption enthalpies for KC_{24}, RbC_{24} and CsC_{24}, plotted as a function of composition.

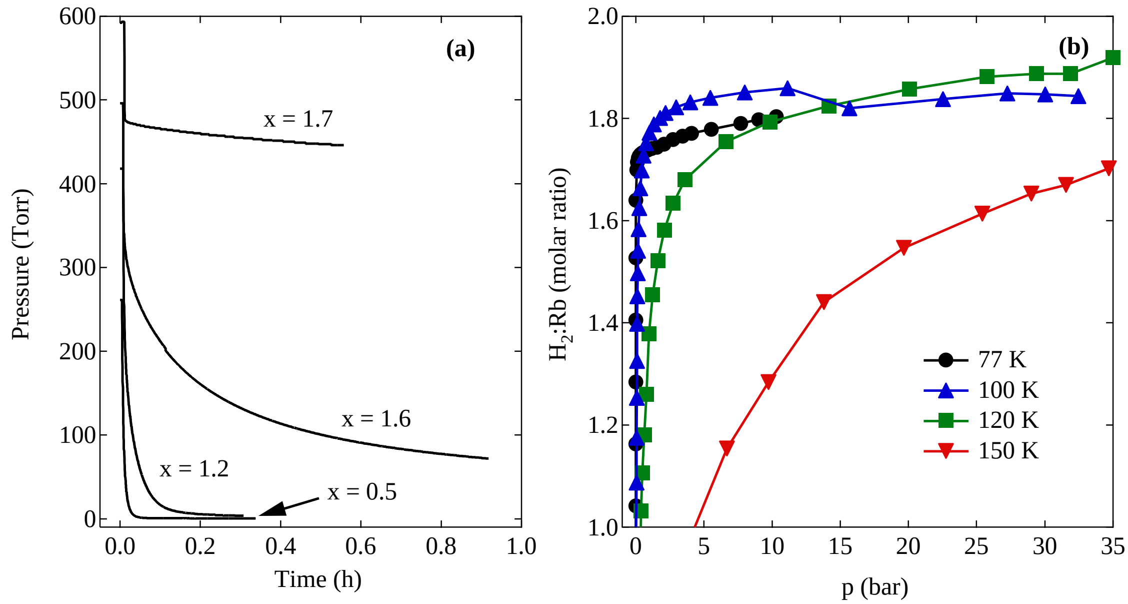

Figure 4.7: Hydrogen adsorption kinetics of RbC_{24}. (a) Manifold pressure is plotted versus time for several compositions at 77 K. Traces are identified by their final composition $RbC_{24}(H_2)_x$. Pressure decreases versus time due to adsorption. (b) Plateau regions of the H_2 adsorption isotherms of RbC_{24} at 77 K, 100 K, 120 K, and 150 K.

(see Sec. 1.4). Of course, it would have been very interesting to measure the adsorption at room temperature to determine the delivery between 3 bar and 100 bar. Unfortunately, the RbC_{24} and CsC_{24} samples also appear to react with hydrogen at 195 K and higher temperatures. Experimentally, we observe a reduction in the maximum 77 K hydrogen adsorption capacity following adsorption at 195 K. A summary of maximum H_2 adsorption capacities and average isosteric heats for KC_{24}, RbC_{24}, and CsC_{24} is listed in Table 4.1.

4.4 Hydrogen adsorption kinetics

Kinetic limitation of adsorption appears to be significant in KC_{24} (as well as in RbC_{24} and CsC_{24}) at hydrogen compositions greater than $x = 1.5$. There are few vacant adsorption sites for the H_2 molecules to diffuse through, leading to site-blocking and correlation effects. Combined with the small jump attempt frequency which exists at these low temperatures, the result is a reduction in the transport-diffusivity of the adsorbed hydrogen phase. Adsorption kinetics were measured for RbC_{24} at 77 K at various hydrogen compositions, as illustrated in Fig. 4.7a. The manifold pressure is plotted versus time for several different final compositions. At low H_2 compositions (e.g., $x = 0.5$) the adsorption is rapid, and the equilibrium pressure is reached within a minute or two. At higher H_2 compositions (e.g., $x = 1.6$) the adsorption is extremely sluggish, and equilibrium is still not reached after an hour. Diffusion-limited adsorption is more significant at low temperatures due to the lower jump attempt frequency. This is evident in Fig. 4.7b, where the 77 K isotherm actually drops below the 100 K isotherm near $x = 1.7$ because the slower adsorption kinetics reduces the adsorption amount that is measured within a specific time (15 min in this case).

4.5 Discussion

Comprehensive measurements of the adsorption enthalpies and adsorption kinetics of the MC_{24} compounds (for M = K, Rb, Cs) were collected over the entire H_2 composition range. The H_2 binding enthalpies for all three compounds are summarized in Fig. 4.6. Compared to activated carbons, there appears to be less energetic heterogeneity in the adsorption potentials of the MC_{24} compounds. The isosteric heats are relatively flat, in contrast to the monotonically decreasing isosteric heats for activated carbons (see Fig. 3.3). Because the MC_{24} compounds have more long-range order than activated carbons, it is intuitive that they would have fewer distinct adsorption sites. In addition, the interlayer spacing is wide enough to accept only a single layer of H_2 molecules, further restricting the distribution of distinct adsorption sites. A positive correlation between the adsorption enthalpy and the interlayer spacing is clearly illustrated in Fig. 4.6. The wider 5.9 Å slit pores of CsC_{24} have a stronger adsorption potential than the narrower 5.4 Å slit pores of KC_{24}. However, this trend may also be affected by differences in the electrostatic interaction, due to varying degrees of charge transfer between the graphite and alkali metals. As listed in Table 4.1, there is also a negative correlation between alkali metal size and adsorption capacity. This is expected, due to the decrease in free volume within the interlayer galleries that occurs with larger alkali metal atoms.

Geometry appears to play a significant role in the sluggish adsorption kinetics observed at large H_2 compositions. Intra-crystalline diffusion in KC_{24} is two-dimensional, which means that site-blocking and correlation effects can be even greater due to the reduction in the number of nearest-neighbor sites. Adsorption kinetics, however, is a macroscopic transport phenomenon which can depend on both inter- and intra-crystalline diffusion as well as surface impurities. It is possible that using flake graphite starting material with smaller particle sizes may improve kinetics, but this was not investigated. It was found that Grafoil-based KC_{24} samples had significantly slower adsorption rates than the flake graphite samples. This may have been due to surface impurities blocking H_2 entry at the crystallite surface. A study of microscopic hydrogen self-diffusion within KC_{24} is presented in Sec. 5.4, and is largely consistent with the slow macroscopic adsorption kinetics measured here.

4.6 Conclusion

Pressure-composition-temperature diagrams were measured for hydrogen adsorption in the intercalated graphite samples KC_{24}, RbC_{24}, and CsC24. Adsorption capacities and isosteric heats were determined and are summarized in Table 4.1. A model-independent, virial-type thermal equation was used to calculate isosteric heats from the experimental isotherms. Consistent with the literature, the KC_{24} isotherm has an “S” shape due to lattice expansion associated with H_2 adsorption [48, 49]. The isosteric heat is positively correlated with the size of the alkali metal intercalant. Hydrogen adsorption is kinetically-limited at large H_2 compositions.